Journal of Nuclear Materials 399 (2010) 146–153

Contents lists available at ScienceDirect

Journal of Nuclear Materials

journal homepage: www.elsevier.com/locate/jnucmat

Transmission electron microscopy study on neutron irradiated pure iron and RPV model alloys

M. Hernández-Mayoral *, D. Gómez-Briceño

CIEMAT, Departamento de Tecnología, División de Materiales Estructurales, Avenida Complutense, 22, 28040 Madrid, Spain

ARTICLE INFO

Article history:
Received 17 July 2008
Accepted 16 November 2009

ABSTRACT

The radiation induced microstructure was examined by Transmission Electron Microscopy in Fe, FeCu, FeMnCuNi, FeMnNi and a Reactor Pressure Vessel steel that were neutron irradiated to 0.026, 0.051, 0.10 and 0.19 dpa at 300 °C. The effect of dose and composition on defect accumulation and microstructure evolution was investigated. The damaged microstructure consisted in the presence of dislocation loops of interstitial type. The presence of voids was also studied in pure iron. Results on density, size and Burgers vector of radiation induced dislocation loops showed that the evolution of the interstitial component of the neutron irradiation induced microstructure was strongly affected by the presence of solutes such as Cu, Mn and Ni. Density and size increased with increasing dose in all the materials, while the effect of solutes is clearly to decrease the size of defects compared to pure iron. It has been observed that, for the same irradiation dose, the defect size decreases as the material becomes more complex, with the extreme case of the RPV steel where no defects were observed at any of the irradiation doses studied.

1. Introduction

Changes in mechanical properties of Reactor Pressure Vessel (RPV) steels in nuclear reactors are the consequence of changes produced at microstructural level under the effect of neutron irradiation. Radiation embrittlement in these materials is attributed to three main microstructural aspects induced by irradiation: matrix damage, copper rich precipitates and segregation to grain boundaries [1–4]. Matrix damage includes both interstitial and vacancy point defect clustering. These clusters, together with Cu rich precipitates, are obstacles to the movement of dislocations under stress, reducing ductility and increasing yield stress, and contribute to increase the probability of brittle fracture. The precipitates of copper are a major contribution to the hardness increase and have been the focus of many experimental and theoretical studies on binary Fe–Cu alloys and steels under various conditions [5–14] However, the relevance of matrix component of damage and of the presence of other solutes can be high in low copper content alloys and also in the case of high fluences [15,16].

The work presented in this paper was performed within the frame of the PERFECT Project, an integrated project funded by the 6th framework programme of EC. The general objective of this project was the construction of a predictive tool based on multiscale modelling techniques. To ensure the reliability of such a tool, the experimental validation of computational codes is required. With that purpose, a neutron irradiation experiment was designed to obtain both an understanding of the basic and relevant mechanism that take place under irradiation, and quantitative experimental data adequate to perform the experimental validation of prediction tools based on multiscale modelling, which are developed in parallel within the same project.

This article is one of three papers devoted to the presentation of experimental results obtained by means of Tomographic Atom Probe (TAP), Small Angle Neutron Scattering (SANS) and Transmission Electron Microscopy (TEM) applied to the same set of neutron irradiated Fe based alloys and to an RPV steel. The results presented here come from TEM characterisation and are complementary to the results coming from the other characterisation techniques reported in companion papers. The relevance of TEM studies in this field stems from its ability to detect the interstitial component of damage, which is a part of radiation damage not detected with other microstructural characterisation techniques in such a direct way. Therefore, TEM results combined with those of complementary techniques, will allow a complete description of the microstructure produced by irradiation in the materials under study to be obtained.

2. Experimental methodology

Different model alloys with similar composition to RPV steels were neutron irradiated at the test reactor BR2 of the SCK·CEN laboratory in Belgium. The materials considered for TEM examination are listed in Table 1. Experimental details regarding radiation

* Corresponding author. Tel.: +34 91 346 66 18; fax: +34 91 346 66 61.
E-mail address: m.mayoral@ciemat.es (M. Hernández-Mayoral).

0022-3115/$ - see front matter © 2009 Elsevier B.V. All rights reserved.
doi:10.1016/j.jnucmat.2009.11.013

Table 1
Neutron irradiated materials.

Material	Nominal composition (wt.%)/impurities
Pure Fe	<30 ppm C
Fe–0.1%Cu	0.1 Cu (<30 ppm C)
Fe–0.3%Cu	0. 3 Cu (<30 ppm C)
Fe–Mn–Ni	1.2 Mn, 0.7 Ni (<30 ppm C)
Fe–Mn–Ni–Cu	1.2 Mn, 0.7 Ni, 0.1 Cu (<30 ppm C)
RPV steel	0.135 C, 0.009 S, 0.013 P, 0.04 Si, 0.37 Mn, 0.69 Ni, 0.13 Cr, 0.52 Mo, 0.065 Cu

conditions and material characteristics as well as the microstructure previous to irradiation are reported in [17]. In particular, the average grain size in pure Fe was 250 μm, and decreased for the rest of the model alloys, specifically, 125 μm for Fe–0.1Cu and 177 μm for Fe–0.3Cu, while for FeMnNi and FeCuMnNi it was 88 μm. The dislocation density ranged from 3.2 up to 9×10^{13} m^{-2}.

The microstructure previous to irradiation of the non-irradiated RPV steel is shown in Fig. 1. The ferritic matrix presented regions with a high density of carbides precipitated near regions almost free of precipitates. These precipitates were placed at grain and subgrain boundaries forming internal groups, and showing a preferential orientation. Some precipitates showed globular morphology and others an elongated morphology. In addition, it was possible to observe, usually at regions with low density of carbides, the presence of small needle shaped Mo rich precipitates. The dislocation density of the material was highly heterogeneous.

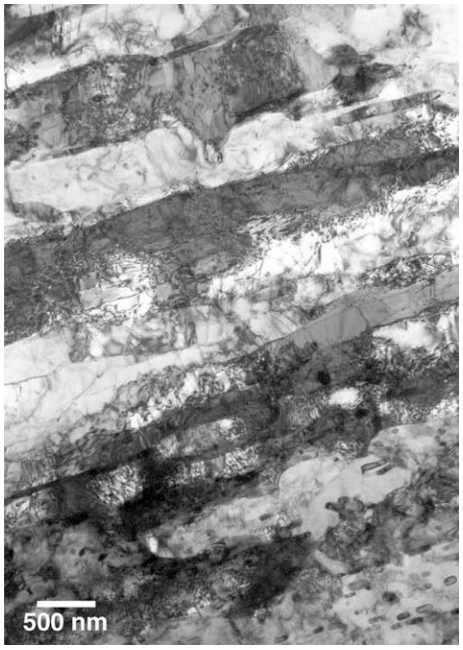

Fig. 1. Microstructure of the RPV steel before neutron irradiation.

The irradiation of different types of specimens was carried out at the reactor operating temperature, 280 °C ⩽ T ⩽ 300 °C. In the present paper, a study by TEM on the effect of dose from 0.026 to 0.19 dpa, at a neutron flux of 0.95×10^{14} n/cm^2 s, is reported. It is worth mentioning that the flux level in these experiments is high compared to the one received by the vessel wall in commercial nuclear reactors and this fact should be taken into account when comparing the resultant microstructures. The effect of flux on microstructure and behaviour of RPV steels is an issue stil under discussion, but the use of high flux allows high dose levels representative of these received by pressure vessel steels after long term operation to be reached.

Table 2 summarises the experimental conditions studied by TEM. The trend of the microstructure evolution has been studied in terms of defect density and defect size, as a function of dose. The examination of model alloys serves to discern the effect of alloying or impurity elements such as Cu, Mn and Ni.

Specimens for TEM were irradiated in the form of 3 mm diameter discs and 100 μm thickness. Special small boxes were fabricated where seven TEM specimens of every material per irradiation condition were placed for their irradiation in the test reactor as explained in [17]. Once exposed to the reactor environment, the specimens were received at CIEMAT laboratories for TEM examination. Irradiated samples were thinned by conventional electropolishing with a Metalthin machine with 5% perchloric acid in methanol at −60 °C. At least two samples per condition and material were examined.

The characterisation of the irradiated microstructure was performed in a JEOL, JEM-2010 Transmission Electron Microscope (TEM) operating at 200 keV, at CIEMAT laboratories. A combination of Bright Field (BF) and Weak Beam Dark Field (WBDF) diffraction contrast conditions were employed to characterise defects induced by neutron irradiation [18,19]. From TEM images, quantitative information was obtained about the density and size of defects. The counting of defects was performed on TEM images recorded under reflections type $g = (1, 1, 0)$, where the best contrast was obtained. No correction was performed on density to take into account that some families of loops are not visible under the reflections used. Therefore, the data presented provide qualitative information on the trend observed for dose effect on defect density. The local thickness needed to calculate density was estimated using the Convergent Beam Electron Diffraction (CBED) method [20].

The dislocation loop size was obtained from TEM images. The method employed was to measure the larger dimension of the loop image. Size distributions are presented in the form of histograms and the average size has been calculated by fitting histograms to a lorentzian function.

The presence of voids was studied by means of a BF through-focal series recorded with the foil tilted away from the Bragg condition for all reflections. Under these conditions, voids appear as white dots surrounded by a dark Fresnel fringe in underfocus images, and as dark dots surrounded by a bright fringe in overfocus images. This method allows voids as small as 1 nm to be detected using defocus values of about 1 μm [18,19].

Table 2
Irradiation conditions (marked with x are those studied by TEM).

Dose	Fe	Fe0.1Cu	Fe0.3Cu	FeMnNi	FeMnNiCu	RPV steel
0026 dpa (1.7×10^{19}n/cm^2)	x	x	x	–	–	x
0051 dpa (3.5×10^{19}n/cm^2)	x	x	x	–	–	x
0,1 dpa (6.9×10^{19}n/cm^2)	x	x	x	x	x	x
0,19 dpa (1.3×10^{20}n/cm^2)	x	x	x	x	–	x

Flux: 0.95×10^{14} n/cm^2 s.

3. Results

3.1. Defect density and size distribution

The series of TEM images in Fig. 2 shows the effect of dose on the microstructure evolution of pure Fe neutron irradiated at 300 °C in a range of dose from 0.026 to 0.19 dpa. The damage produced by neutron irradiation was in the form of directly observable defects at all the dose levels studied. They were identified as small dislocation loops which are visible as white dots under WBDF conditions or black dots under two beam BF imaging conditions at low doses, 0.026 and 0.051 dpa. Defect clusters observed after 0.1 dpa and 0.19 dpa clearly showed the typical contrast of dislocation loops under the different reflection conditions employed. These

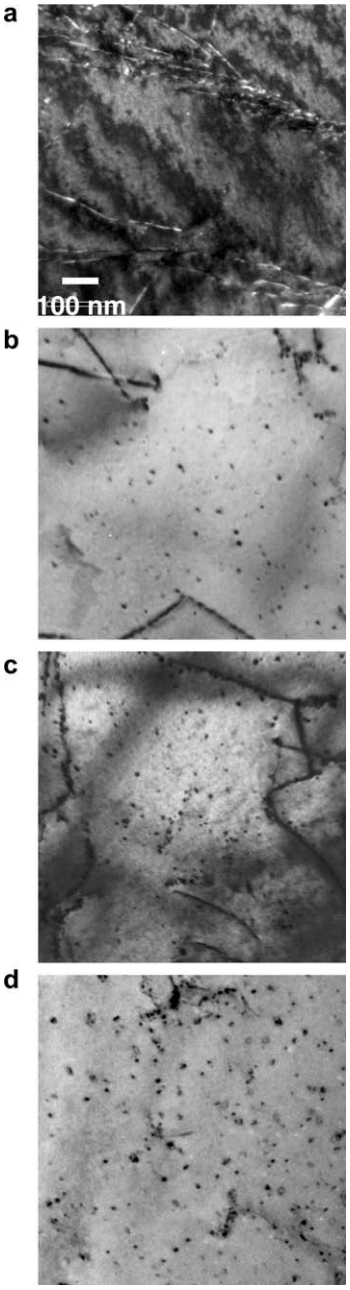

Fig. 2. Microstructure of pure Fe, after neutron irradiation up to (a) 0.026 dpa, (b) 0.051 dpa, (c) 0.1 dpa and (d) 0.19 dpa at 300 °C.

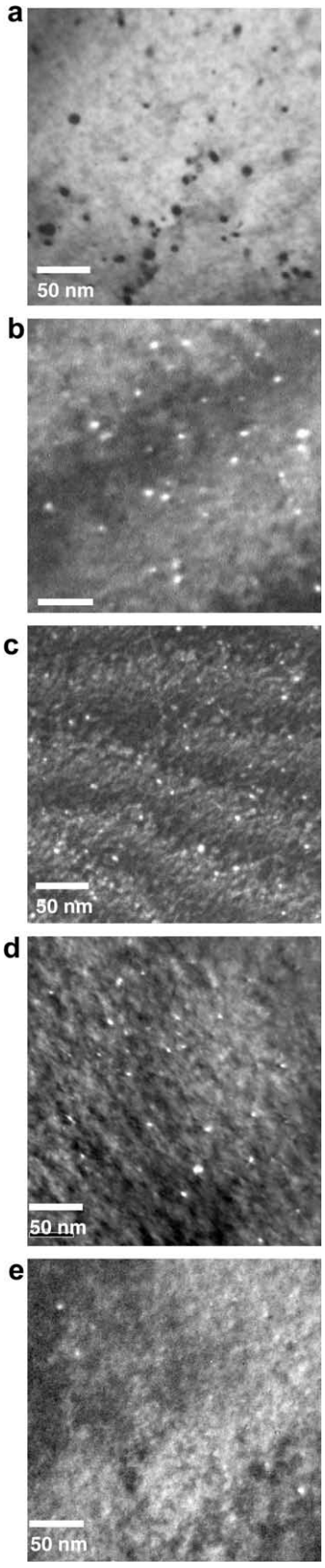

Fig. 3. TEM images showing microstructure induced by neutron irradiation at 0.1 dpa and 300 °C in (a) Fe, (b) Fe–0.1Cu, (c) Fe–0.3Cu, (d) FeMnNiCu and (e) FeMnNi.

Table 3
Summary of quantitative results obtained from TEM images.

Material	Dose (dpa)	Average size (nm) (total number measured loops)	Maximum size (nm)	Density ($\times 10^{20}$ dislocation loops/m^{-3})
Fe	0.026	–	–	3.4 ± 0.4
	0.051	4.9 ± 0.3 (251)	15	8.6 ± 0.8
	0.10	7.1 ± 0.2 (663)	21	12.8 ± 0.8
	0.19	10.2 ± 0.3 (1721)	49	39.1 ± 0.7
Fe–0.1Cu	0.026	–	–	5.8 ± 0.6
	0.051	–	–	2.8 ± 0.3
	0.10	4.5 ± 0.1(1690)	22	11.8 ± 0.8
	0.19	7.7 ± 0.2 (888)	31	19.0 ± 0.9
Fe–0.3Cu	0.026	–	–	–
	0.051	–	–	3.4 ± 0.5
	0.10	5.2 ± 0.2 (848)	19	34.7 ± 0.6
	0.19	7.2 ± 0.2 (1736)	26	51.3 ± 0.6
FeCuMnNi	0.026	–	–	–
	0.051	–	–	–
	0.10	3.2 ± 0.2 (53)	8	10.7 ± 0.7
	0.19	–	–	–
FeMnNi	0.026	–	–	–
	0.051	–	–	–
	0.10	3.9 ± 0.1 (32)	7	4.00 ± 0.4
	0.19	4.7 ± 0.2 (395)	21	9.6 ± 0.8

defects were distributed homogeneously in the matrix, though in some cases dislocation decoration was also observed. Visible loops increased in size with dose but no overlap was observed in this dose range (see Fig. 2).

The neutron damage microstructure found in FeCu, FeCuMnNi and FeMnNi alloys, was qualitatively similar to what has been described above for pure Fe. FeMnNi was examined after 0.1 and 0.19 dpa, and FeCuMnNi after 0.1 dpa. Defects caused by neutron irradiation were observed at all conditions studied, except at the lowest dose (0.026 dpa) in Fe–0.3Cu. Fig. 3 shows a series of images

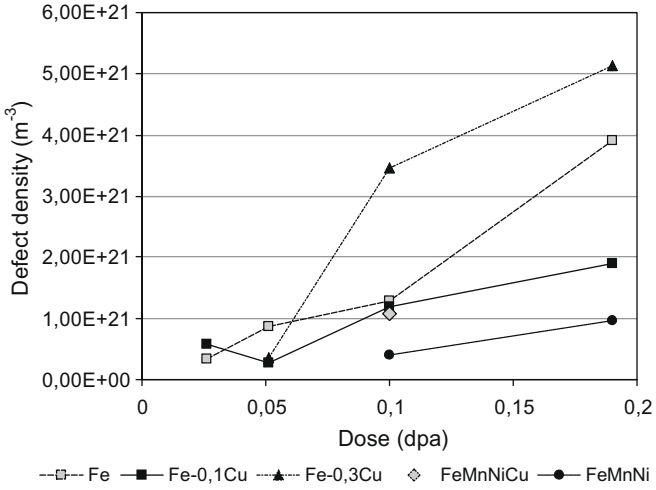

Fig. 4. Dose dependence of visible defect cluster density in neutron irradiated RPV model alloys at 300 °C.

comparing neutron induced microstructure for all model alloys at 0.1 dpa, 300 °C. Regarding the RPV steel, after irradiation the same ferritic microstructure was observed with a similar carbide distribution as before irradiation: globular and elongated precipitates heterogeneously distributed at the ferritic matrix. No defects that could be attributed to neutron exposure were observed, in particular, no dislocation loops were observed at any of the considered doses.

From TEM images, quantitative information was obtained regarding density and size distribution of defects which is summarised in table 3. The density of visible dislocation loops as a function of dose is shown in Fig. 4 for all the model alloys studied. Defect density increases when dose increases from 0.026 to

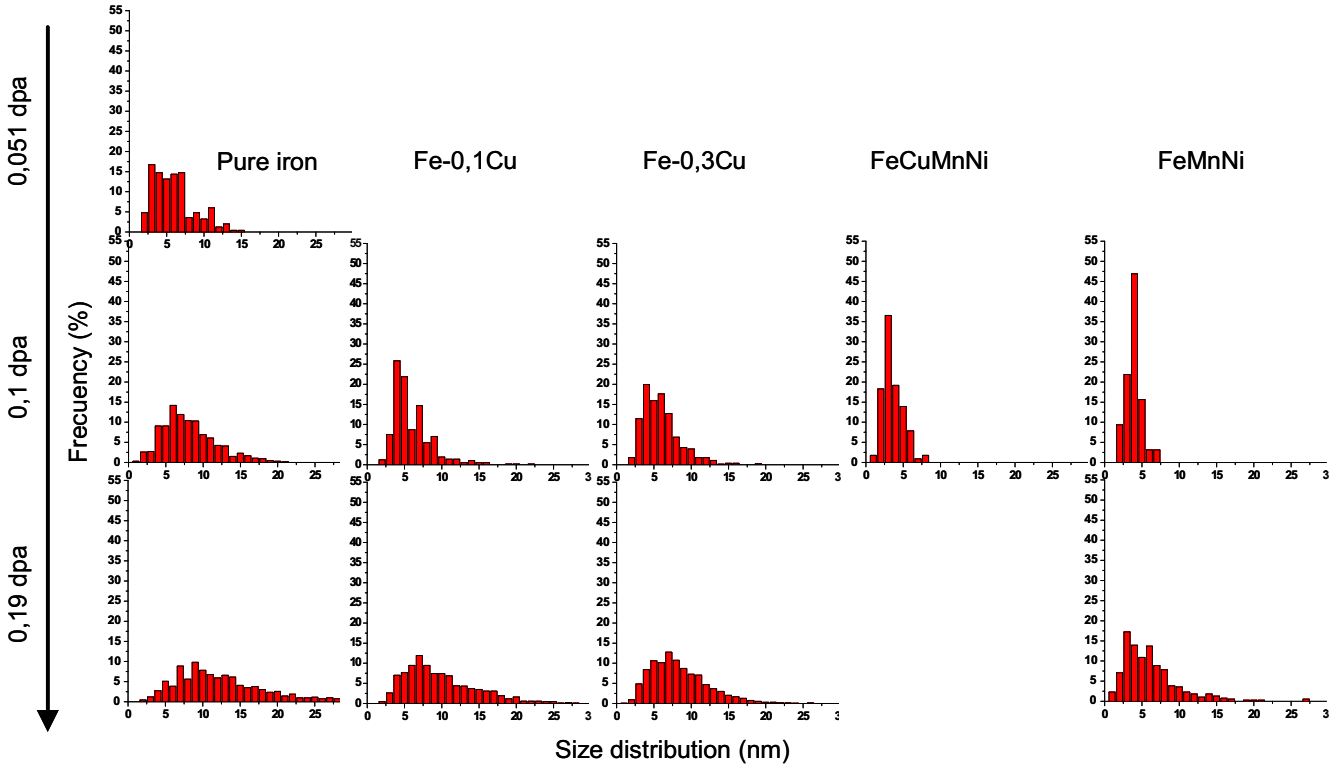

Fig. 5. Histograms showing size distribution of defects in neutron irradiated RPV model alloys at 300 °C, at different doses.

0.19 dpa, in pure iron. For the model alloys an increase of defects with density is also observed, although the trend can not be clearly deduced, due to either scatter in the data or in the number of data points for that material. In all cases, no saturation of the defect density was observed at these dose levels. Fe–0.3Cu shows higher density than pure iron except at 0.051 dpa where a lower density was found, a fact that can be related to the bad quality of these particular specimens that reduced visibility of defects. However, Fe–0.1Cu shows a similar density as pure iron, except at higher doses, where it shows lower density. Only FeMnNi clearly shows lower density than pure iron. As mentioned above, the values of defect densities must be considered as qualitative, since no corrections for those families of loops that are not visible were included.

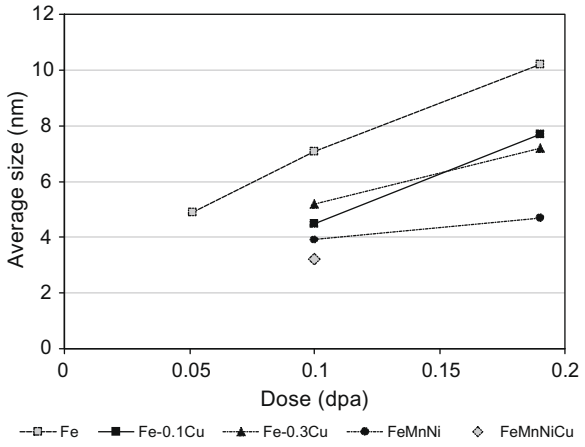

Fig. 6. Dose dependence of average size of dislocation loops in neutron irradiated RPV model alloys at 300 °C.

Defect size distributions are presented in Fig. 5 in the form of histograms for different doses and materials. A clear effect of dose on size distribution is observed. Histograms become broader as dose increases in all the materials, and maximum and mean size increase with dose. In addition, a clear effect of the composition on size distribution is observed. The size distribution becomes narrower in both Fe–Cu alloys compared to pure iron, being the effect more pronounced in the case of FeCuMnNi and FeMnNi alloys, where the lowest average sizes and the narrowest size distributions are obtained. The average size dependence on dose for every material is shown in Fig. 6. The trends in defect size are clear, namely, the effect of dose is to increase the average size for pure Fe and the rest of model alloys, while the effect of composition is to decrease size as the system becomes more complex.

3.2. Loop morphologies

The loop Burgers vector, b, has been determined in pure Fe, Fe–0.1Cu and Fe–0.3Cu alloys irradiated up to 0.19 dpa, where large loops were observed. The invisibility criterion of dislocation loops under specific diffraction conditions was employed [18,19]. Fig. 7 shows an example of two BF images taken on the same area in irradiated pure Fe, under reflections $g = (2, 0, 0)$ and $g = (0, -1, 1)$ near pole [1 1 0]. Table 4 shows values of the $g\,b$ product for the analysis performed, where $g\,b = 0$ means that the dislocation loop shows no contrast, therefore it is invisible under the reflection employed to form the image. From the table it can be deduced that those loops showing no contrast under $g = (2, 0, 0)$ reflection, but visible under $g = (0, -1, 1)$ are of type [0 1 0] or [0 0 1]. Those dislocation loops visible under both reflections would be two families of type 1/2

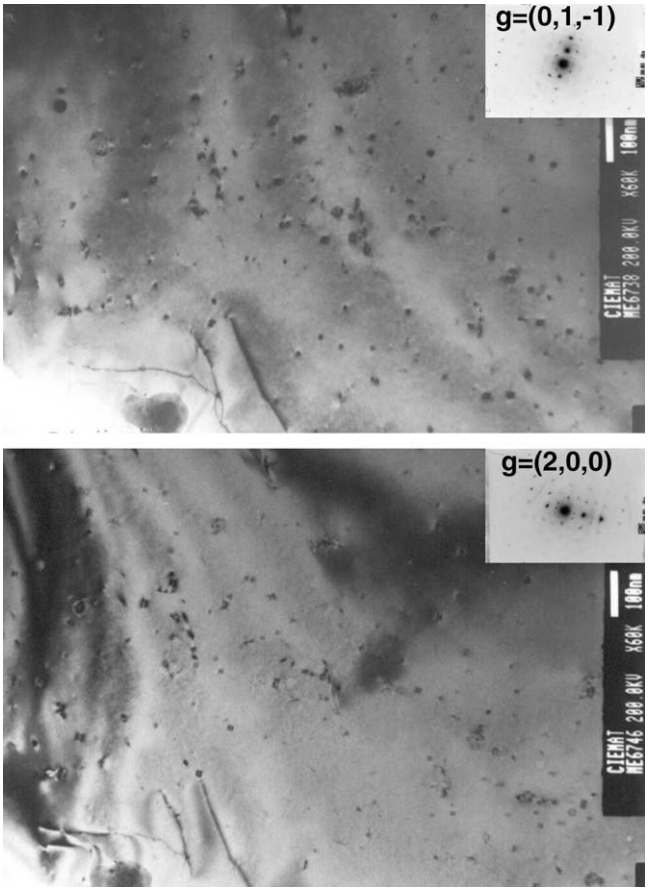

Fig. 7. Burgers vector analysis in pure Fe neutron irradiated at 0.19 dpa, 300 °C.

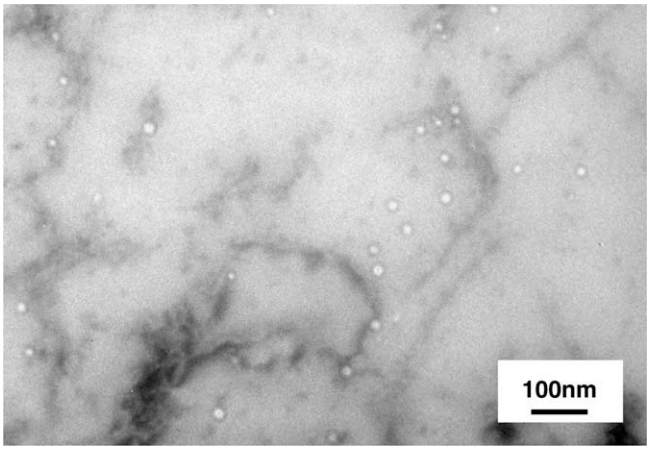

Fig. 8. Underfocused TEM image showing the presence of large voids in pure Fe neutron irradiated at 0.19 dpa, 300 °C.

Table 4
g·b product values for reflections near [1 1 0] pole for the Burgers vector type expected in Fe and RPV model alloys.

g/b	1/2[1 1 1]	1/2[−1 1 1]	1/2[1 −1 1]	1/2[1 1 −1]	[1 0 0]	[0 1 0]	[0 0 1]
(0, 1, −1)	0	0	1	1	0	1	1
(2, 0, 0)	1	1	1	1	2	0	0

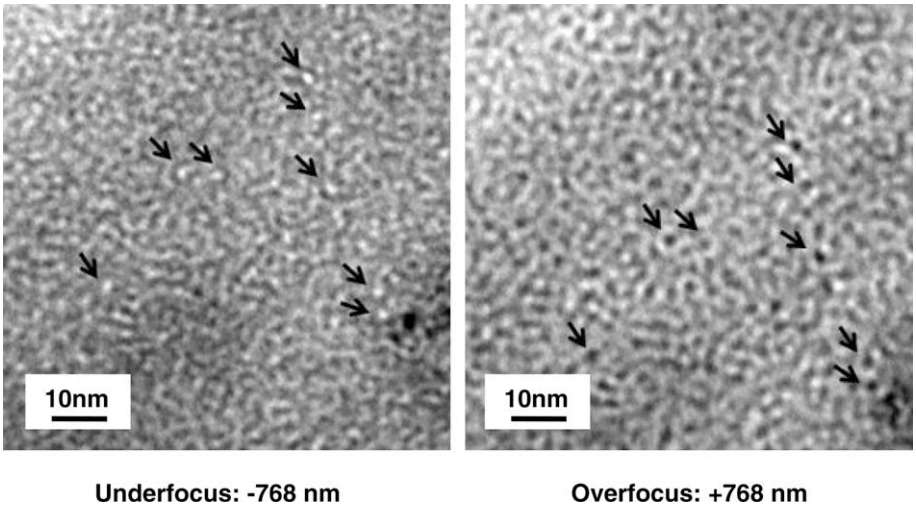

Fig. 9. TEM images of voids in Fe neutron irradiated to 0.19 dpa at 300 °C (a) underfocused and (b) overfocused conditions. The arrows point to several possible small voids.

⟨1 1 1⟩. Finally, b of those loops visible under $g = (2, 0, 0)$ and invisible under $g = (0, -1, 1)$ cannot be discerned, namely, it is not possible to say if they are type 1/2 ⟨1 1 1⟩ or ⟨1 0 0⟩. By comparing images in Fig. 7 under both reflections and similar ones in different areas, it has been obtained that out of a total of 174 loops, 150 loops were visible under $g = (0, -1, 1)$ and not under $g = (2, 0, 0)$, so 86% of the loops had Burgers vector of type ⟨1 0 0⟩, 10% of type b = 1/2 ⟨1 1 1⟩, while the remaining 4% can be either 1/2 ⟨1 1 1⟩ or ⟨1 0 0⟩. Although the Burgers vector is known for the majority of the dislocation loops, the additional information needed to discern about the vacancy or interstital nature of the observed dislocation loops could not be obtained.

In Fe–0.1Cu, following the same procedure as in pure iron, it was concluded that most of the loops were of type ⟨1 0 0⟩, with similar proportion of ⟨1 0 0⟩ or 1/2 ⟨1 1 1⟩ loops as in pure Fe. Finally, in Fe–0.3Cu, it was again obtained that the majority of defects have Burgers vector type ⟨1 0 0⟩. In this case, a slight increase in 1/2 ⟨1 1 1⟩proportion was observed as 63% of defects had b = ⟨1 0 0⟩, 20% had 1/2 ⟨1 1 1⟩ and 17% remain undetermined.

3.3. Voids

Pure Fe neutron irradiated to 0.19 dpa at 300 °C was examined to study the presence or not of voids. An investigation is underway to assess this issue in the rest of irradiation conditions and materials. Large voids with an average size of (12 ± 0.4) nm and an estimated density of 1.2×10^{20} m^{-3}, were observed as shown in Fig. 8. Also the presence of smaller voids was investigated and arrows in Fig. 9 point to features tentatively identified as small voids, with sizes of about 2 nm. These observations suggest the presence of a bimodal distribution of vacancy clusters. Large and small voids appear to be randomly distributed throughout the grain interior. In particular, they were not observed to appear preferentially associated to dislocation loops.

4. Discussion

4.1. Damage accumulation in pure iron

The effect of neutron irradiation observed by TEM has been the production of defect clusters in the form of dislocation loops. In pure Fe at 300 °C and 0.19 dpa, the majority of loops had Burgers vector type ⟨1 0 0⟩. It is thought this is also the case at lower doses in agreement with other results found in the literature, for similar irradiation temperatures, but lower doses, 0.04 [21] and 0.07 dpa [22,23]. Interstitial or vacancy nature of dislocation loops could not be determined here, but they are most probably interstitial type according to previous TEM studies on neutron irradiated pure iron, where this fact was determined either directly [24,25] or indirectly by in situ annealing [21] or electron irradiation [26]. However, the fact that a fraction of the smaller dislocation loops could be of vacancy type [27] is not discarded, though it is not probable that the large vacancy clusters collapse to planar configurations according to simulation results [28,29] where the minimum energy structures of pure vacancy clusters are, in general, spherical in shape.

In this work, vacancy clusters in the form of large and small voids have been observed in pure Fe at 0.19 dpa and 300 °C. Similar large voids were observed by Horton [24] at 300 °C and 1 dpa in pure Fe, and small voids are reported to have been detected by Positron Annihilation Spectroscopy (PAS), and also by TEM [30]. According to molecular dynamics simulations [31,32] the damage produced in collision cascades in Fe consists of self-interstitial atom (SIA) and vacancies, that are mostly isolated or form very small clusters. The irradiation temperature used in the experiment presented here is above Stage III for Fe and close to Stage V, therefore vacancies are able to migrate at these temperatures, and small clusters of vacancies are probably able to dissociate. This can result in a high supersaturation of vacancies that could give rise to the growth of larger and more stable vacancy clusters at the expense of the single vacancies and smaller clusters. This would explain the presence of small voids observed here. However, the occurrence of spherical clusters of sizes such as those observed in these experiments (~12 nm) still needs to be understood. In other materials, the existence of voids is associated to the presence of gas such as He produced by transmutation due to the neutron irradiation [30], as He could stabilize these vacancy clusters into spherical voids. However, the production rate of He under neutron irradiation conditions considered here is thought to be very low.

Regarding evolution with dose of the interstitial component of damage in pure iron, dislocation loop density is observed to increase with dose up to 0.19 dpa. Defect clusters have been observed from the lower dose considered, 0.026 dpa (1.7×10^{19} n/cm^2). Their observation by TEM implies that the growth of interstitial clusters take place after the formation of interstitials at the outshell of cascades, reaching TEM observable sizes (above 1.5 nm in diameter). In pure iron, it is unlikely they cluster and reach TEM observable sizes directly in the cascade. For the highest recoil energies modelled by molecular dynamics simulations in

this material with recently developed interatomic potentials, the maximum SIA cluster size has less than 20 defects [32,33], clearly below the resolution of TEM. However, it must be taken into account that the simulation times are very short, only of a few picoseconds. Another aspect to consider, regarding evolution of SIA clusters, is the particular dislocation loop configuration they reach in terms of their Burgers vector. As mentioned above, in pure Fe, most of the loops observed were of ⟨1 0 0⟩ type and reached sizes about 10 nm at the highest dose, 0.19 dpa. The mechanism of formation of these loops is still an unresolved issue because calculations show as the most energetically favourable configurations the ⟨1 1 0⟩ or 1/2 ⟨1 1 1⟩. The last ones are energetically more favourable for clusters containing more than five defects, both according to empirical potentials and based on *ab initio* calculations [34,35]. Hence, some kind of interaction or transformation of smaller⟨1 1 0⟩ or 1/2 ⟨1 1 1⟩ should occur to produce the large ⟨1 0 0⟩ dislocation loops that are found experimentally in this and other works [21–24]. The formation of ⟨1 0 0⟩ loops through the interaction of ⟨1 1 1⟩ loops has been proposed as a possible mechanism, based on molecular dynamics simulations [36]. However, recent experiments by Arakawa et al. [37] suggest the direct transformation of ⟨1 1 1⟩ loops into ⟨1 0 0⟩ loops during annealing at 300 °C. Therefore, once SIA have been formed at the outshell of cascades during irradiation, they can diffuse and grow by random encounters with other SIA clusters or free interstitials forming clusters with dislocation loop configuration, first ⟨1 1 0⟩ and then larger as ⟨1 1 1⟩, but still too small to be observable by TEM. As irradiation proceeds, these small loops can transform to ⟨1 0 0⟩ by processes such as the one observed by Arakawa [37] and also grow to reach larger cluster sizes than those obtained from individual cascade simulations and, consequently, reaching visible TEM sizes. Some dislocation loops type 1/2 ⟨1 1 1⟩ also have the chance to grow to observable sizes with no transformation, as a fraction of them are observed in these experiments. The experimental results presented here show that SIA clusters grow as dose accumulates from 0.026 dpa. The growth of existing clusters occurs together with the generation of new ones because a population of defects with size at the resolution limit of TEM, 1.5–2 nm, is always observed. Therefore, these experimental results reveal that the dominant processes in microstructural evolution, in this dose range, are nucleation and growth of self-interstitial clusters.

4.2. Copper effect

In both Fe–Cu alloys studied in this work the observed effect of dose was similar to what has been explained above for pure iron, namely, dislocation loop density and size increase with increasing dose. The presence of Cu in iron reduces cluster size, this means that the presence of copper in iron reduces the rate of growth of interstitial clusters being necessary a higher dose to reach a similar size to that in pure iron. The influence of Cu on SIA cluster evolution could be explained by a direct binding between Cu and SIA or SIA clusters, but *ab initio* calculations show that the interaction between Cu and SIA is very weak and the formation of a mixed dumbbell is very unfavourable [38]. Thus, a direct interaction between Cu and SIA is not believed to be the prevalent mechanism to affect evolution of SIA clusters under irradiation in FeCu model alloys. An indirect effect of Cu on SIA clustering through Cu-vacancy interactions can then be considered. In Fe containing Cu, an association of vacancies with Cu atoms forming Cu-vacancy complexes has been found experimentally by PAS [11]. A strong binding between Cu and vacancies has also been obtained using *ab initio* simulations [39]. This binding will result in a higher effective migration energy of vacancies in Fe–Cu alloys than in pure Fe, thus affecting vacancy diffusion and enhancing recombination with SIA, possibly at Cu-vacancy sites, decreasing the number of interstitials available for cluster growth, hence reducing interstitial cluster growth rate.

The formation of Cu-vacancy complexes and their interaction with SIA clusters seems to affect also the morphology of dislocation loops and an increase of the proportion of 1/2 ⟨1 1 1⟩ loops compared to pure iron at 0.19 dpa and 300 °C was observed. This result was already reported by Ebrahimi et al. [22] for Fe–0.3% Cu content compared to pure Fe at lower dose, 0.04 dpa. It is possible that this fact results from the influence of Cu atoms on interstitial cluster mobility. Calculations using empirical potentials for Fe–Cu [40] have shown that for the case of ⟨1 1 1⟩ clusters moving one-dimensionally (clusters with 10 defects or more), Cu acts as an obstacle for this one-dimensional motion, reducing their trajectories and decreasing their diffusivity. The loss of mobility would allow the growth of these 1/2 ⟨1 1 1⟩ loops and the achievement of visible TEM sizes, increasing their observed proportion in FeCu model alloys in comparison with pure Fe.

In the same manner Cu, through its association with vacancies, affects evolution of interstitial clusters, it is possible that interstitial clustering affects also the mechanisms of Cu redistribution in the matrix under irradiation as simulation results from Barashev et al. [41] point out. This fact would imply that interstitial component of irradiation damage should be taken into account to explain evolution processes leading to solute redistribution in matrix due to irradiation, Cu in this case. The study of the possible mechanisms for copper precipitation using simulations has been mostly focused on the vacancy component of damage and its interaction with Cu atoms [42]. Recently, calculations are starting to include a possible interaction between SIA and Cu atoms [40,43] as well as with other solutes [39], but independently from the vacancy component. The results obtained here by TEM regarding the interstitial component of the damage indicate that it is necessary to take into account the concurrent production and evolution of vacancies and self-interstitials in the presence of Cu to describe in a consistent form the changes in the microstructure of these materials.

4.3. Mn and Ni effect

FeMnNiCu and Fe–0.1Cu alloy have similar copper content and they can be compared at 0.1 dpa. Both alloys presented a similar defect density, but there is a clear difference on size distribution of defects, being narrower and with smaller average size for the alloy containing Ni and Mn. Regarding the free copper alloy, FeMnNi, showed the lowest density among all the alloys. Size distribution is also narrower than in pure Fe and Fe–Cu alloys, being similar to FeMnNiCu alloy. These results point to the fact that Ni and Mn atoms limit loop growth in these alloys, as much narrower size distribution than in alloys with no Ni or Mn is observed. Hence, TEM results reflect a possible interaction of Mn and Ni atoms with interstitial point defects or clusters. In the case of Mn, this fact is in agreement with results from *ab initio* calculations where Mn shows a preference to bind to SIAs than to vacancies [39].

From the results presented, it is concluded that as alloy composition becomes more complex, the size of interstitial clusters observed by TEM decreases compared with pure iron, showing that the processes undertaken under irradiation by this type of defects are influenced by material composition. As the size of clusters decrease, an important fraction could have a size under TEM resolution limit that could explain part of the observed decrease in defect density in FeMnNi alloys.

4.4. RPV steel

Finally, in the RPV steel no defects that could be attributed to neutron irradiation could be observed by TEM. This result agrees

with the fact observed on model alloys: as materials become more complex, defect clusters created by irradiation decrease in size falling below TEM resolution limit. In addition, it is worth to point out that the microstructure of real steels is complex, with a high density of dislocations, martensite lath boundaries and precipitates that could act as sinks for point defects. Part of the defects created by neutron irradiation can disappear in such structures before being able to group and form clusters large enough to be observed by TEM.

5. Conclusions

A study by TEM has been carried out to investigate the effect produced by neutron irradiation on the microstructure of pure Fe, Fe0.1Cu, Fe0.3Cu, FeMnNiCu and FeMnNi and an RPV steel. The main results obtained are:

- Dislocation loops have been observed in all the materials except in the RPV steel. Density and size of defects increased with increasing dose up to the highest dose level studied, 0.19 dpa.
- The majority of dislocation loops had Burgers vector type ⟨1 0 0⟩ and are considered to be interstitial in nature according to previous studies [21–25].
- Voids have been observed in pure iron at 0.19 dpa and 300 °C.
- Copper addition has a clear effect on size distribution of interstitial clusters, being narrower than in pure iron, and decreasing its average and maximum size compared to pure iron. This means that the growth rate of interstitial clusters decreased.
- Copper in pure iron has an influence on Burgers vector type of dislocation loops, and the percentage of $b = 1/2\ \langle 1\ 1\ 1\rangle$ loops increases for Fe–0.3Cu compared to pure iron.
- The addition of Mn and Ni narrows the size distribution and average size of interstitial clusters, and this fact implies an interaction among solute atoms and radiation induced point defects of interstitial type, leading to a reduction in growth rate of interstitial clusters.
- As materials become more complex, those defects created by the irradiation are reduced in size falling below TEM resolution. In the RPV steel studied, the same microstructure was observed before and after irradiation. No defects were observed that could be attributed to the neutron irradiation; particularly, no dislocation loops were found. This result is consistent with the systematic observation of reduced defect size in model alloys with solute content.

The results presented constitute a set of experimental data obtained under well-known and well-controlled experimental conditions. It is also a systematic study of damage evolution as a function of composition. These results provide relevant information about the microstructure produced under irradiation by neutrons. Mechanisms have been proposed to explain the processes observed that take place under irradiation of pure iron and model alloys. In combination with the other techniques employed to study the same materials by other researchers (TAP and SANS) a complete picture of the damage generated by neutrons will emerge. This extensive data will be of fundamental importance to validate the experimental methods that are being currently developed to produce a predictive model of irradiation effects in RPV steels.

Acknowledgements

This work was supported within the European Integrated Project PERFECT under Contract No. F16O-CT-2003-508840. The authors wish to thank Mr. J. L. Mozo Polo for his assistance in TEM sample preparation and Dr. M. J. Caturla for helpful and clarifying discussions.

References

[1] G.R. Odette, G.E. Lucas, Radiat. Eff. Defects Solids 144 (1–4) (1998) 189–231.
[2] W.J. Phythian, C.A. English, J. Nucl. Mater. 205 (1993) 162–177.
[3] G.R. Odette, Scr. Metall. 17 (1983) 1183–1188.
[4] Y. Nishiyama, K. Onizawa, M. Suzuki, J.W. Anderegg, Y. Nagai, T. Toyama, M. Hasegawa, J. Kameda, Acta Mater. 56 (16) (2008) 4510–4521.
[5] R.G. Carter, N. Soneda, K. Dohi, J.M. Hyde, C.A. English, W.L. Server, J. Nucl. Mater. 298 (2001) 211–224.
[6] K. Fukuya, K. Ohno, H. Nakata, S. Dumbill, J.M. Hyde, J. Nucl. Mater. 312 (2003) 163–173.
[7] M.K. Miller, M.G. Burke, J. Nucl. Mater. 195 (1992) 68–82.
[8] M.K. Miller, B.D. Wirth, G.R. Odette, Mater. Sci. Eng. A 353 (2003) 133–139.
[9] M.k. Miller, K.F. Russell, J. Nucl. Mater. 371 (2007) 145–160.
[10] P. Auger, P. Pareige, S. Welzel, J-C. Van Duysen, J. Nucl. Mater. 280 (2000) 331–344.
[11] Y. Nagai, Z. Tang, M. Hassegawa, T. Kanai, M. Saneyasu, Phys. Rev. B, 63, (2001), 134110.
[12] P. Asoka-Kumar, B.D. Wirth, P.A. Sterne, R.H. Howell, Philos. Mag. Lett. 82 (11) (2002) 609–615.
[13] S. Jumel, J-C. Van Duysen, J. Ruste, C. Domain, J. Nucl. Mater. 346 (2005) 79–97.
[14] G.R. Odette, B.D. Wirth, D.J. Bacon, N.M. Ghoniem, MRS Bull. (March) (2001).
[15] T.J. Williams, D. Ellis, D.I. Swan, J. McGuire, S.P. Walley, C.A. English, J.H. Venables, P.H.N. de la Cour Ray, in: Proceedings of the 2nd International Symposium on Environment Degradation of Materials in Nuclear Power Systems-Water Reactors, ANS, 1986, p. 323.
[16] T.J. Williams, P.R. Burch, C.A. English, P.H.N. de la Cour Ray, in: Proceedings of the 3rd International Symposium on Environment Degradation of Materials in Nuclear Power Systems-Water Reactors, ANS, 1988, p. 121.
[17] A. Almazouzi, K. Verheyen, L. Malerba, M. Hernández-Mayoral, D. Gómez-Briceño, "Characterisation of Neutron Irradiated Samples (REVE matrix)" Interim Report, Integrated Project PERFECT, 2005.
[18] M.L. Jenkins, M.A. Kirk, Characterization of Radiation Damage by Transmission Electron Microscopy, Institute of Physics, Bristol, 2001.
[19] J.W. Edington, Practical Electron Microscopy in Materials Science, Macmillan Philips Technical Library, 1975.
[20] M.H. Loretto, Electron Beam Analysis of Materials, Chapman and Hall Ltd, 1984.
[21] A.C. Nicol, M.L. Jenkins, M.A. Kirk, Mater. Res. Soc. Symp. Proc. 50 (2000).
[22] F. Ebrahimi, D.T. Hoelzer, D. Venables, V. Krishnamoorthy, Development of a Mechanistic Understanding of Radiation Embrittlement in Reactor Pressure Vessel Steels. Final Report, Department of Materials Science and Engineering, University of Florida, 1988.
[23] D.T. Hoelzer, F. Ebrahimi, Mater. Res. Soc. Symp. Proc. 373 (1995).
[24] L.L. Horton, J. Bentley, K. Farrell, J. Nucl. Mater. 108/109 (1982) 222–233.
[25] I.M. Robertson, M.L. Jenkins, C.A. English, J. Nucl. Mater. 108/109 (1982) 209–221.
[26] M. Horiki, T. Yoshiie, M. Iseki, M. Kiritani, J. Nucl. Mater. 271/272 (1999) 256–260.
[27] B.L. Eyre, A.F. Bartlett, Philos. Mag. 12 (1965) 261–272.
[28] A. Takahashi, N. Soneda, S. Ishino, G. Yagawa, Phys. Rev. B 67 (2003) 024104.
[29] N. Soneda, T. Díaz de la Rubia, Philos. Mag. A 78 (1998) 995.
[30] M. Eldrup, B.N. Singh, J. Nucl. Mater. 276 (2000) 269–277.
[31] R.E. Stoller, G.R. Odette, B.D. Wirth, J. Nucl. Mater. 251 (1997) 49.
[32] N. Soneda, T. Díaz de la Rubia, Philos. Mag. A 81 (2001) 331.
[33] L. Malerba, J. Nucl. Mater. 351 (2006) 28.
[34] C. Björkas, K. Nordlund, Nucl. Instrum. Methods B 259 (2007) 853.
[35] F. Willaime, C.C. Fu, M.C. Marinica, J. Dalla Torre, Nucl. Instrum. Methods B 228 (2005) 92.
[36] J. Marian, B.D. Wirth, J.M. Perlado, Phys. Rev. Lett. 88 (2002) 255507.
[37] K. Arakawa, K. Ono, M. Isshiki, K. Mimura, M. Uchikoshi, H. Mori, Science 318 (2007) 956.
[38] C. Domain, C.S. Becquart, Phys. Rev. B 65 (2001) 024103.
[39] E. Vincent, C.S. Becquart, C. Domain, J. Nucl. Mater. 359 (2006) 227–237.
[40] J. Marian, B.D. Wirth, J.M. Perlado, G.R. Odette, T. Díaz de la Rubia, Phys. Rev. B 64 (2001) 094303.
[41] A.V. Barashev, S.I. Golubov, D.J. Bacon, P.E.J. Flewitt, T.A. Lewis, Acta Mater. 52 (2004) 877–886.
[42] J. Marian, B.D. Wirth, G.R. Odette, J.M. Perlado, Comput. Mater. Sci. 31 (2004) 347–367.
[43] F. Christien, A. Barbu, J. Nucl. Mater. 324 (2004) 90–96.